Measurement of antineutrino scattering on free protons in MINERνA

Tejin Cai

York University

GHP2023,
April 14, 2023

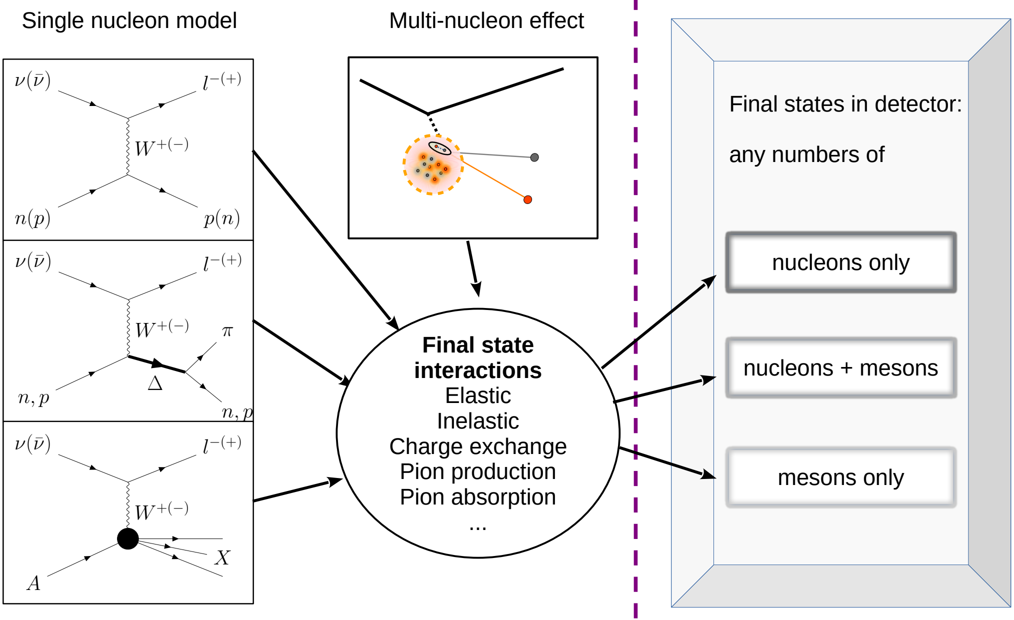
Single nucleon model
Multi-nucleon effect
$\nu(\bar{\nu})$
$l^{-(+)}$
$W^{+(-)}$
$n(p)$
$p(n)$
π
Δ
n, p
A
X
Final state interactions
Elastic
Inelastic
Charge exchange
Pion production
Pion absorption
...
Final states in detector:
any numbers of
nucleons only
nucleons + mesons
mesons only

Nucleon and nuclear effects are inseparable

NuWro
Wrocław Neutrino Event Generator

Genie
UNIVERSAL NEUTRINO GENERATOR
& GLOBAL FIT

Neutrino measurements depend on models.
Most factor out nucleon and nuclear effects:

1. Neutrino-nucleon interactions
2. Fermi motion, binding energy
3. Final state interactions
4. Event kinematics → combine uncertainty from previous steps!

GiBUU
The Giessen Boltzmann-Uehling-Uhlenbeck Project

NEUT

Nucleon form factor impacts oscillation physics

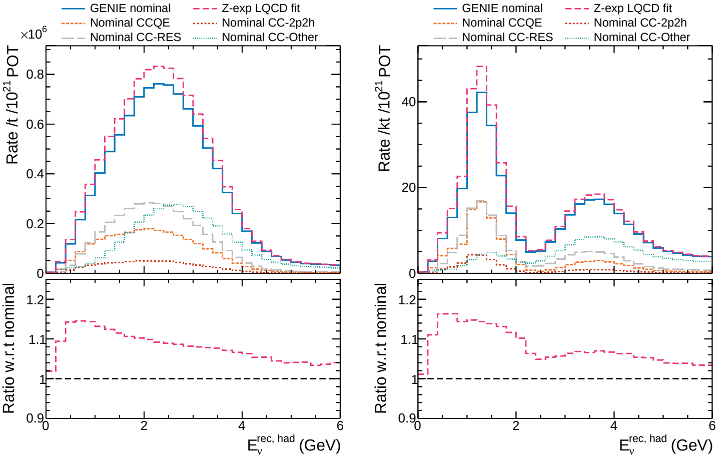

ν_μ event rate in DUNE near (left) and far (right) detector.

$$E_\nu^{\text{rec,had}} = E_l + \sum_p E_{\text{kin}} + \sum_{\pi^\pm,\pi^0,\gamma} E_{\text{tot}}$$

- Solid blue: GENIEv3 10a_02_11a, CCQE uses dipole F_A.
- Dashed black: replace dipole F_A with z-expansion F_A fitted to LatCat LQCD.

$10\% \sim 20\%$ effect.
Meyer, Walker-Loud, and Wilkinson, 2022[1].

Measure the charged current elastic (CCE) scattering

$$\bar{\nu}_\mu + p \to \mu^+ + n,$$

with the Medium Energy NuMI neutrino beam, and the scintillators in MINERνA.

- No nuclear effect on hydrogen.
- Large carbon background.
- POT:1.12×10^{21}
- No. of hydrogen atoms: $\sim 2.61 \times 10^{29}$

There is an equal number of carbon:

- Nuclear effects that alter the kinematics of the outgoing particles.
- Use this fact to constrain this background

MINERνA detector

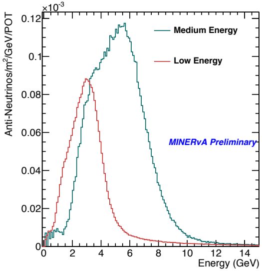

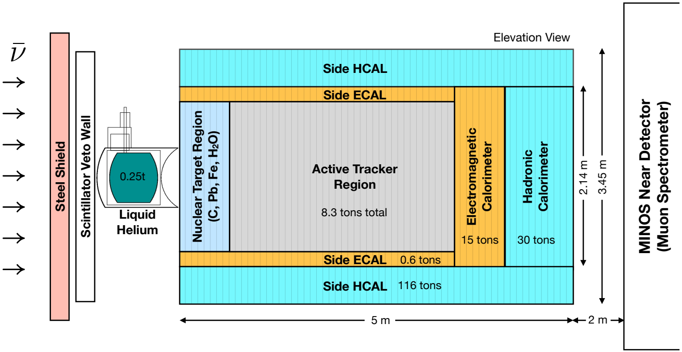

Nucl. Inst. and Meth. A743 (2014) 130.

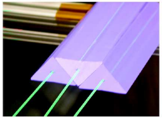

Element	# of Targets
H	2.61×10^{29}
C	2.38×10^{29}

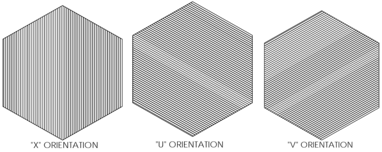

Boost hydrogen fraction with nuclear effects

$\bar{\nu}_\mu H$ is a 2-body process.
Final state neutron kinematics predictable from muon measurement.

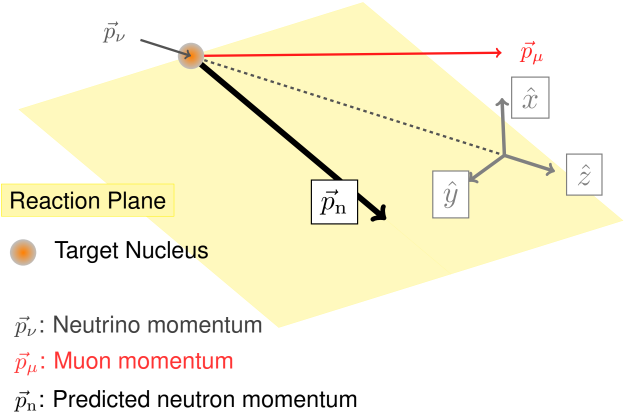

Boost hydrogen fraction with nuclear effects

$\bar{\nu}_\mu H$ is a 2-body process. Final state neutron kinematics predictable from muon measurement.

Fermi motion, nuclear effects, and final state interaction cause neutrons from carbon to deviate.

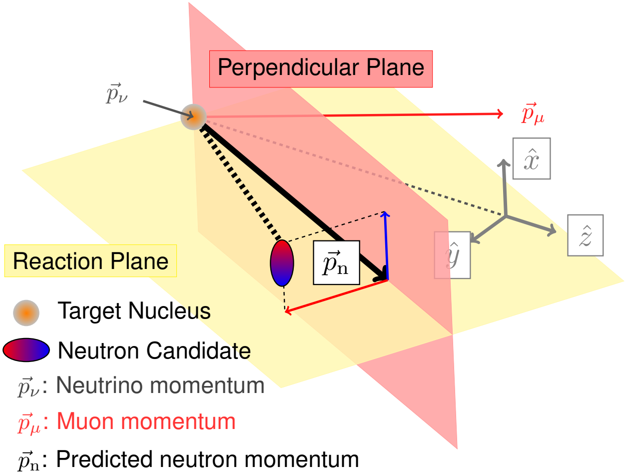

Boost hydrogen fraction with nuclear effects

$\bar{\nu}_\mu H$ is a 2-body process. Final state neutron kinematics predictable from muon measurement.

Fermi motion, nuclear effects, and final state interaction cause neutrons from carbon to deviate.

Capture this deviation in the neutron direction, using $\delta\theta_\mathrm{P}$ and $\delta\theta_\mathrm{R}$

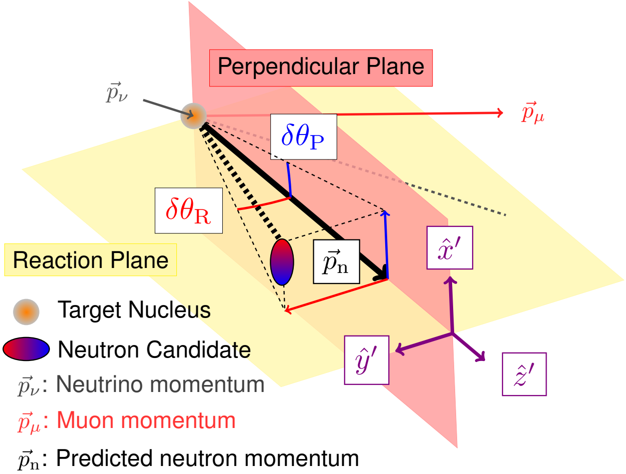

Neutrons inside the detector interact with hydrogen or carbon to produce charged secondary particles.

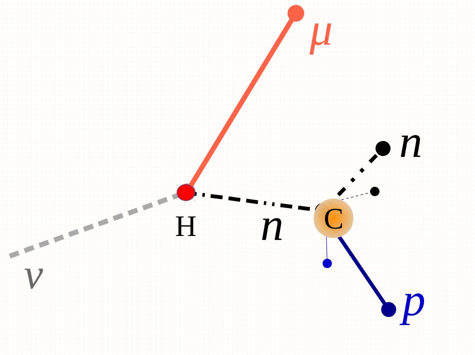

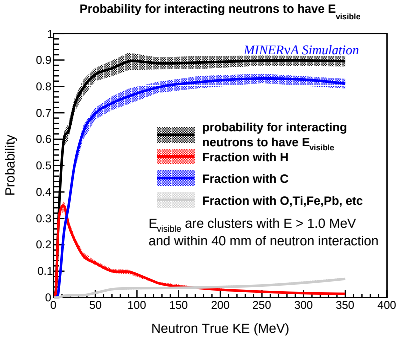

Most prompt neutron energy deposits due to knockout protons.

Neutron signature

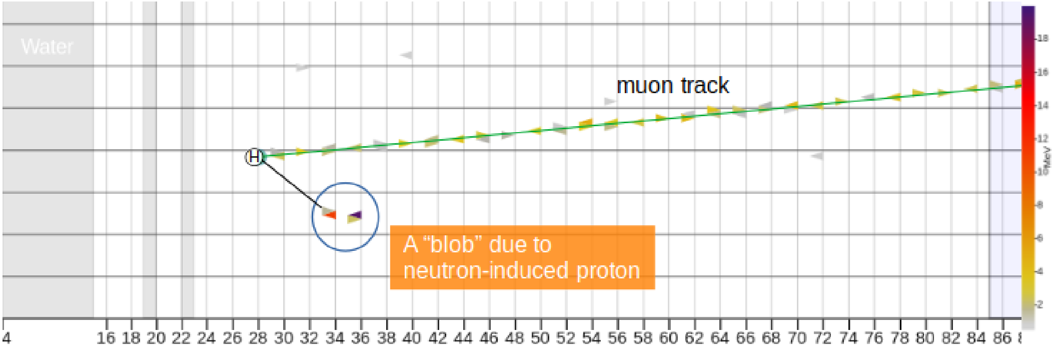

An incoming anti-neutrino scatters off a hydrogen producing neutron. The neutron undergoes secondary interactions to produce visible proton.

Blobbing algorithm

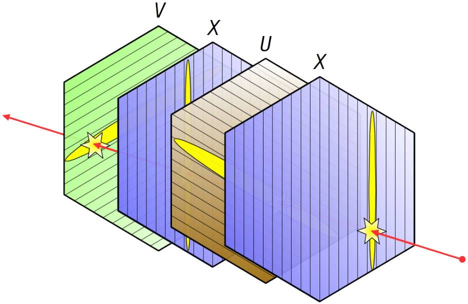

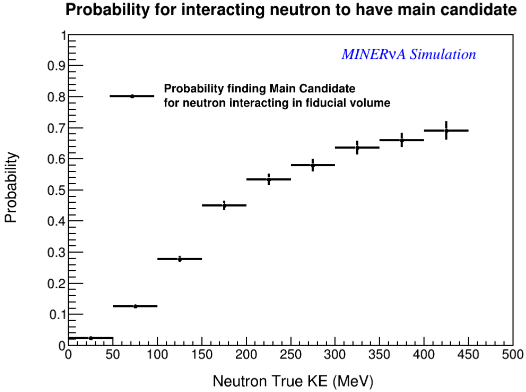

Quasi-elastic like (QELike) event selection

Event topology:

- 1 μ^+ and no reconstructed hadronic track

Neutron selection:

- ≥ 1 three-dimensional neutron candidate
- Leading candidate energy deposited 10 cm away from the muon axis.

Muon acceptance due to detector shape:

- $1.5\ \text{GeV} < E_\mu < 20\ \text{GeV}$
- $\theta_\mu < 20^\circ$ w.r.t. to neutrino beam

NuMI Antineutrino Mode: 1.12×10^{21} Protons on Target

Total recoil energy cut:

Condition	$E^{\text{recoil}}_{\text{max}}$ (GeV)
$Q^2_{\text{QE}} < 0.3\ (\text{GeV}/c)^2$	$0.04 + 0.43 Q^2_{\text{QE}}/(\text{GeV}/c)^2$
$Q^2_{\text{QE}} < 1.4\ (\text{GeV}/c)^2$	$0.08 + 0.3 Q^2_{\text{QE}}/(\text{GeV}/c)^2$
$Q^2_{\text{QE}} > 1.4\ (\text{GeV}/c)^2$	0.50

Angular distribution of events

$\sim 94,000$ events.

Each angular variable is not selective enough → go to two dimensions

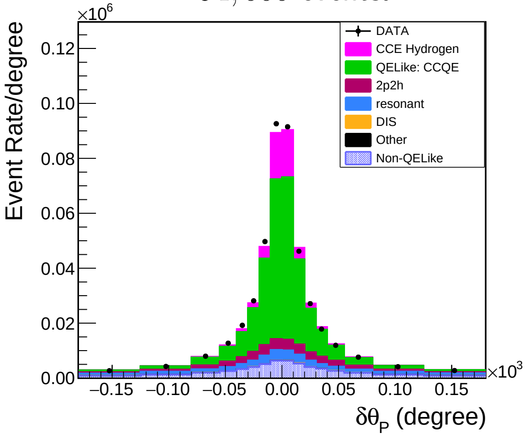

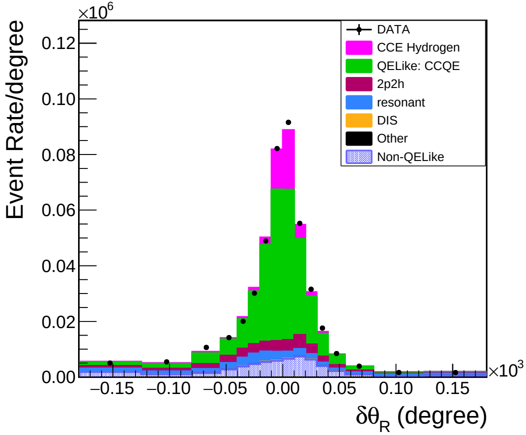

CCE hydrogen QELike CCQE carbon 2p2h

Angular regions and MC fraction

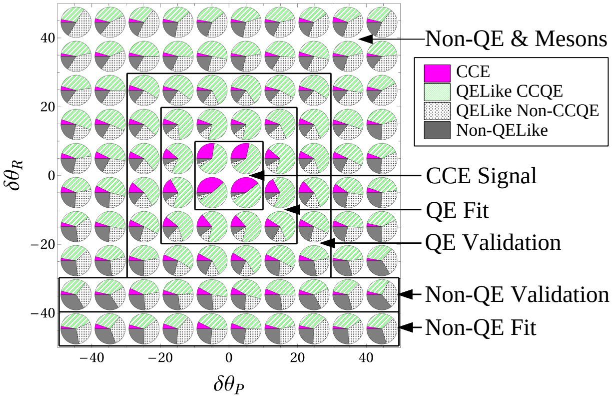

Total data event rate

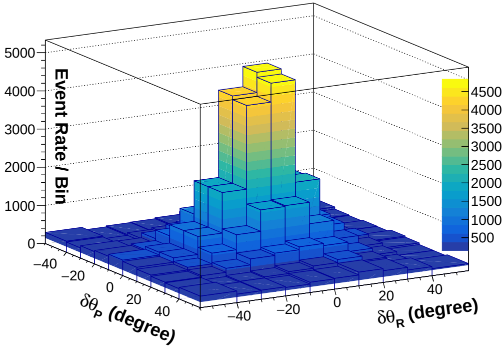

Created different angular regions – Hydrogen signal in the center. Outer regions are used for fit and validation – expand each region in Q^2

Angular regions and MC fraction

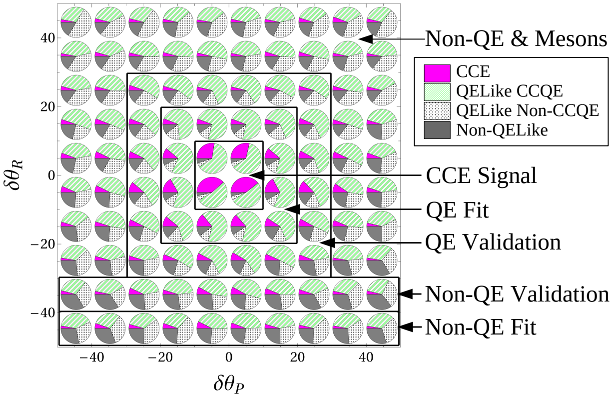

MC events in slices of Q^2

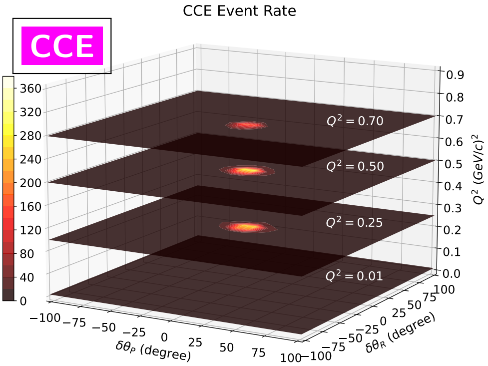

Predicted hydrogen angles – concentrated in the center.

Angular regions and MC fraction

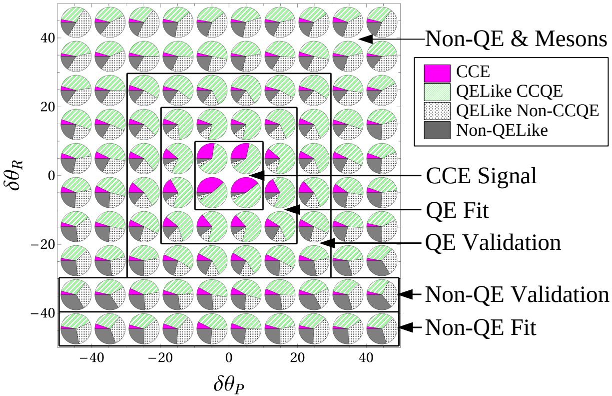

MC events in slices of Q^2

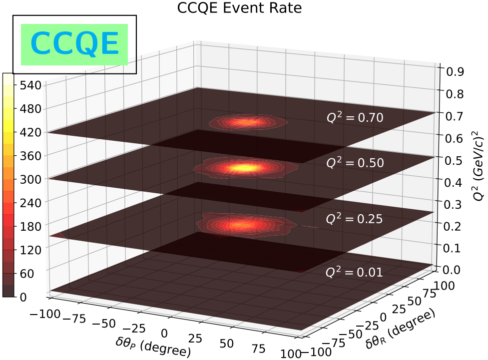

Carbon QELike (CCQE) – more spread out due to Fermi motion and final state interactions.

Angular regions and MC fraction

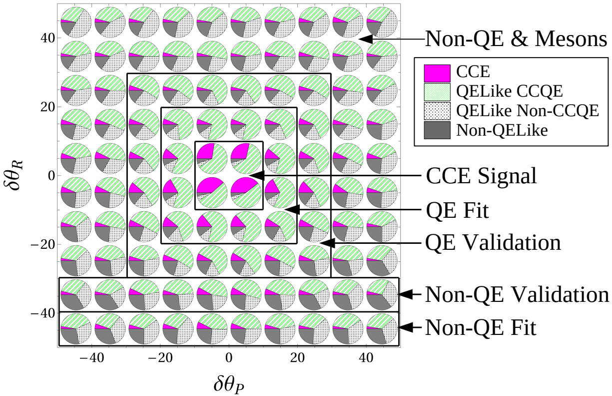

MC events in slices of Q^2

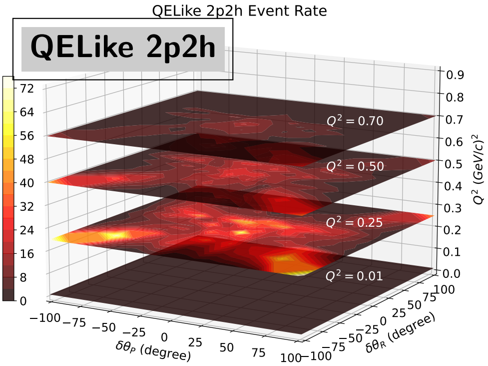

2p2h and resonant – all over the place but different.

Angular regions and MC fraction

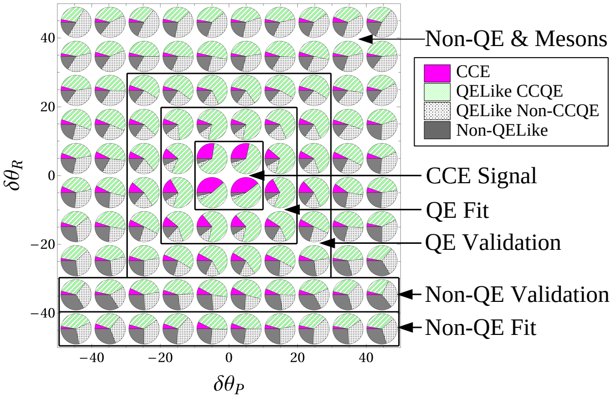

MC events in slices of Q^2

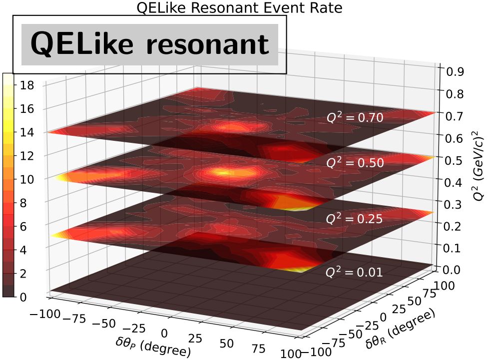

2p2h and resonant – all over the place but different.

Fit using sideband region

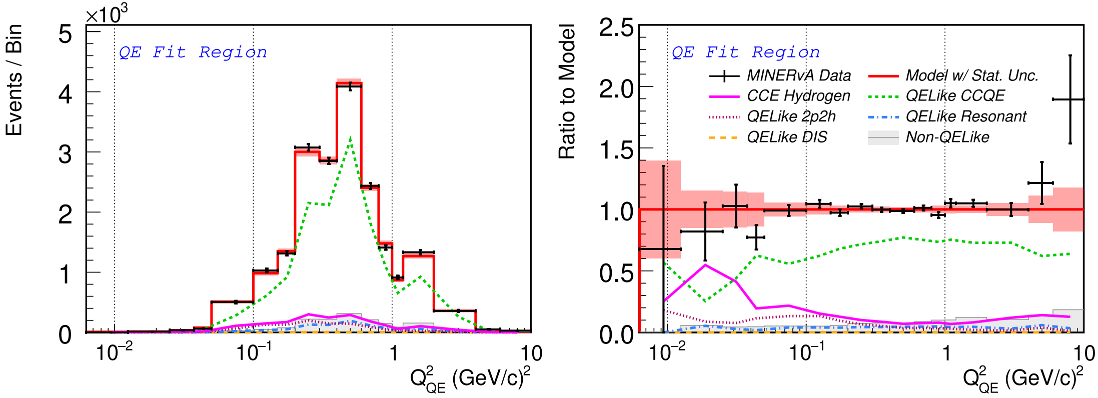

CCQE is the dominant background. Small 2p2h, resonant, and Non-QELike contributions. The fitted model are well constrained by data.

Check fit with validation region

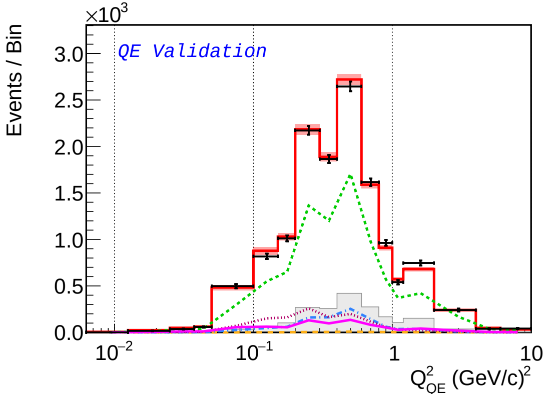

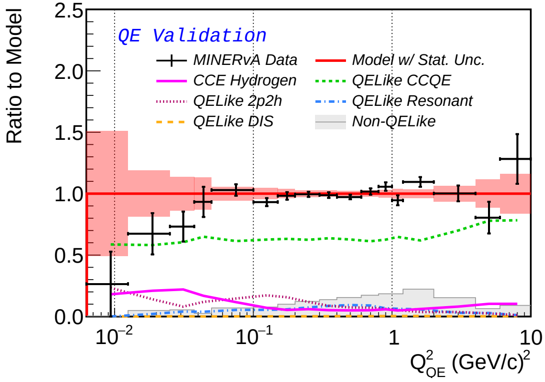

CCQE is the dominant background. Small 2p2h, resonant, and Non-QELike contributions. The fitted model are well constrained by data.

Apply fit to signal region

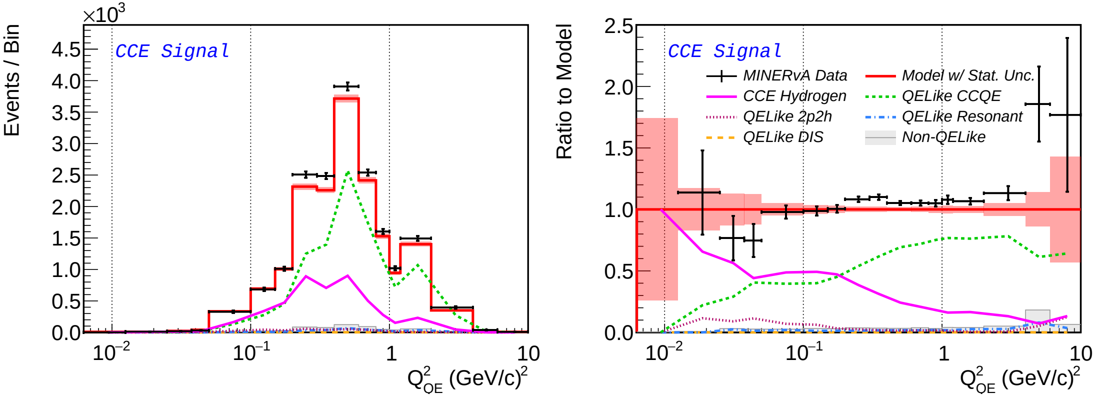

Projecting the fit into the signal region. Difference between data and background is the physics. More than 5000 hydrogen events!

Apply fit to signal region

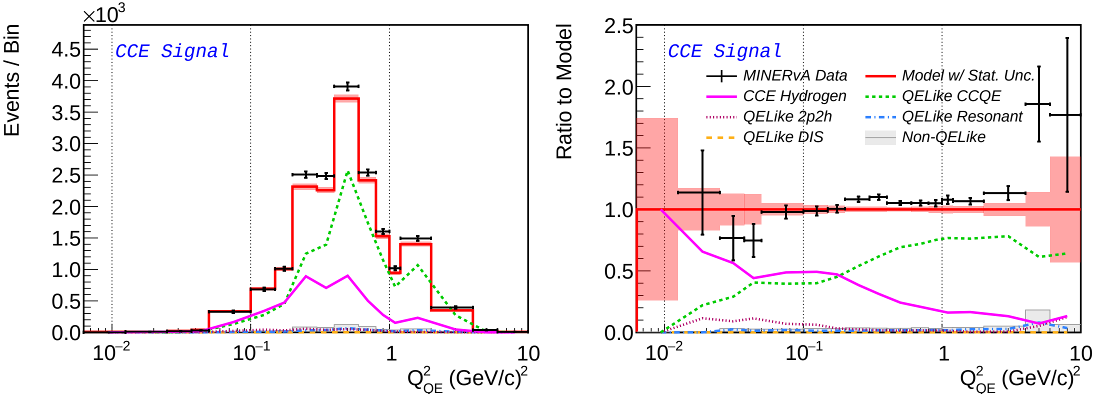

Subtract background, and correct detector smearing using D'Agostini iterative unfolding with 4 iterations.

Efficiency

$$\epsilon = \frac{\texttt{signal events recorded}}{\texttt{total signal events produced}}$$

- Peaks at $Q^2 \sim 0.3\,(\mathrm{GeV}/c)^2$
- Low Q^2: Low acceptance because neutron needs to produce protons that span at least 2 planes.
- high Q^2: Reconstruction inefficiency and larger opening angles and less detector material to contain neutrons.

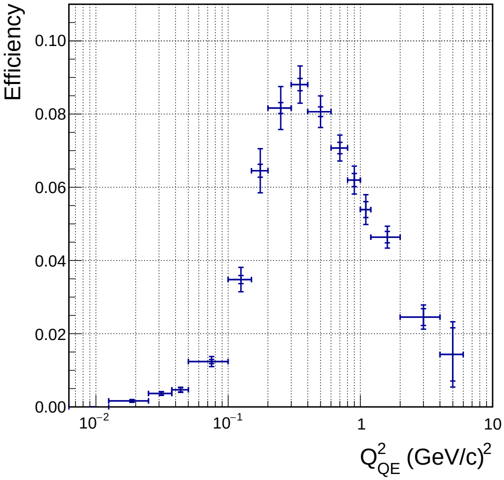

Cross section prediction

- The single nucleon Llewelyn Smith equation convolutes with flux and muon acceptance.
  - Necessary for theory calculations.
- We use a standard vector form factor parameterization. (BBBA2005, Bradford et al., 2005[2])
- F_A fit assumes z-expansion form[3] (details in the backup).

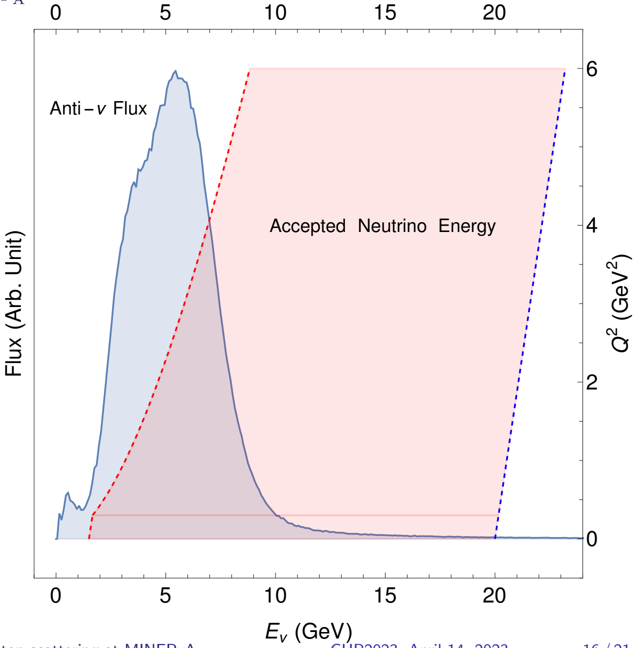

Cross section

Deuterium Fit: Meyer et al., 2016[3]

BBBA2007: Bodek et al. 2007[4]

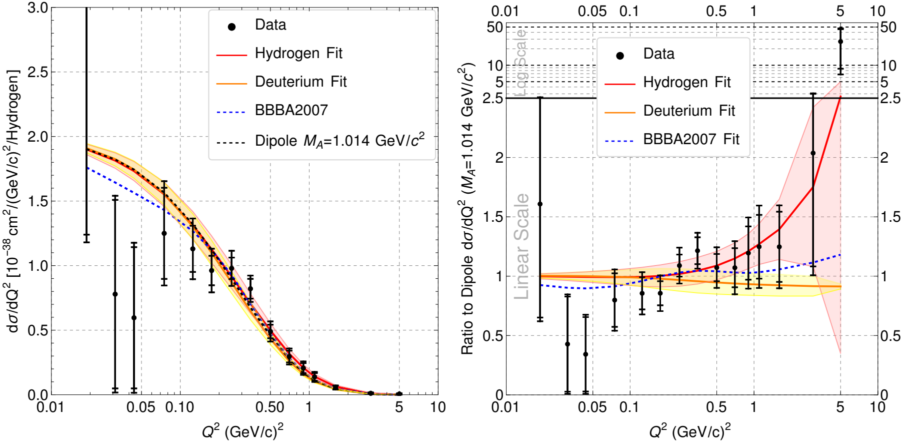

Figure: Extracted cross section and ratio to a dipole form factor.

Systematic and statistical uncertainty

- Dominated by statistical uncertainty from background subtraction, despite enhanced signal
- Systematic uncertainties from residuals of background subtraction
- Particle responses in the "other" category, dominated by neutron systematics.

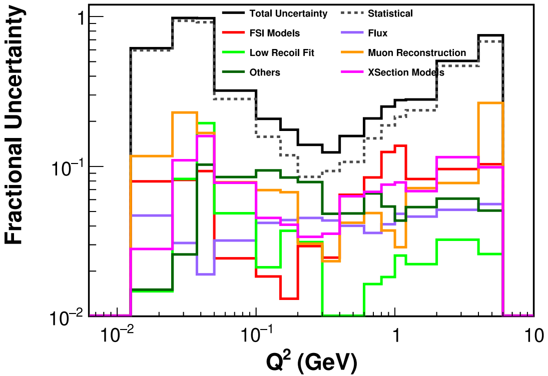

LQCD: Lin 2022[5]

F_A fit and axial radius of the nucleon

Result of F_A fit:

Deuterium fit applies z-expansion to bubble chamber data focused for $Q^2 < 1\,(\mathrm{GeV}/c)^2$. Hydrogen fit data up to $Q^2 = 5\,(\mathrm{GeV}/c)^2$. Tension between hydrogen and deuterium at larger Q^2.

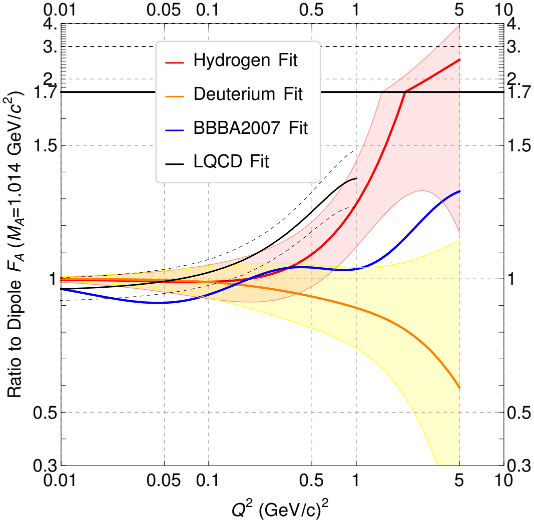

LQCD: Lin 2022[5]

F_A fit and axial radius of the nucleon

Result of F_A fit:

A fit to lattice QCD calculation by Lin[5] is consistent with our fitted F_A up to $1\ (\mathrm{GeV}/c)^2$

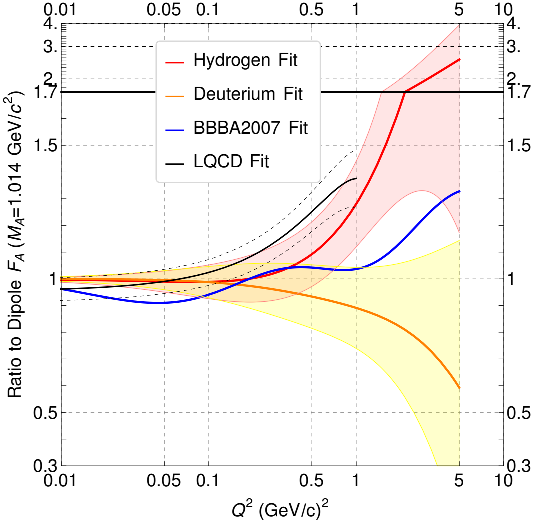

LQCD: Lin 2022[5]

F_{A} fit and axial radius of the nucleon

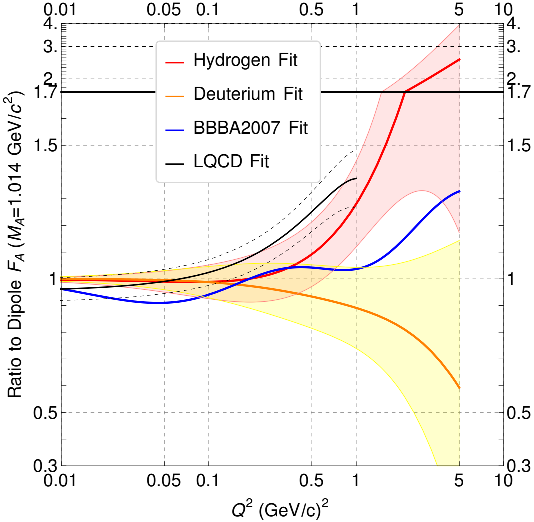

Result of F_{A} fit:

Calculate proton radius from F_{A} for $Q^2 \to 0$.

$$F_{\mathrm{A}}(Q^2) = F_{\mathrm{A}}(0)\left(1 - \frac{\langle r_A^2\rangle}{3!}Q^2 + \frac{\langle r_A^4\rangle}{5!}Q^4 + \dots\right),$$

$$\frac{1}{F_{\mathrm{A}}(0)}\frac{\mathrm{d}F_{\mathrm{A}}}{\mathrm{d}Q^2}\bigg|_{Q^2=0} = -\frac{1}{6}\langle {r_A}^2\rangle$$

- $\langle r_A^2\rangle = 0.53(25)\mathrm{fm}^2$
- $\sqrt{\langle r_A^2\rangle} = 0.73(17)\mathrm{fm}$

LQCD: Lin 2022[5]

F_{A} fit and axial radius of the nucleon

Result of F_{A} fit:

Calculate proton radius from F_{A} for $Q^2 \to 0$.

$$F_{\mathrm{A}}(Q^2) = F_{\mathrm{A}}(0)\left(1 - \frac{\langle r_A^2\rangle}{3!}Q^2 + \frac{\langle r_A^4\rangle}{5!}Q^4 + \dots\right),$$

$$\frac{1}{F_{\mathrm{A}}(0)}\frac{\mathrm{d}F_{\mathrm{A}}}{\mathrm{d}Q^2}\bigg|_{Q^2=0} = -\frac{1}{6}\langle {r_A}^2\rangle$$

- $\langle r_A^2\rangle = 0.53(25)\mathrm{fm}^2$
- $\sqrt{\langle r_A^2\rangle} = 0.73(17)\mathrm{fm}$

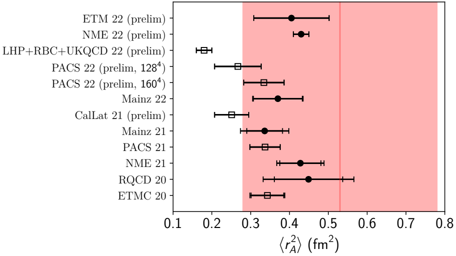

Filled circle: full error budget.
Open square: incomplete.
Red band: this result.
Courtesy of Aaron Meyer.

Summary

Made a new F_A measurement in 30 years and the only statistically significant measurement on free nucleon.

- The result will aid in better understanding the weak nucleon structure.
- An important ingredient for oscillation physics → impacts cross section.
- The new techniques developed are useful for current and future experiments:
  - neutron reconstruction
  - method of background constraint
- Can we reduce uncertainties in future iterations?

Thank you!
The MINERvA Collaboration

Backup

Mann et al., 1973[6]

First neutrino - deuterium measurement

Reported exactly 50 years ago:

- Flux uncertainty was 15%
- Extracting form factor needs model-dependent deuterium corrections
  - Fermi motion
  - Pauli exclusion principle

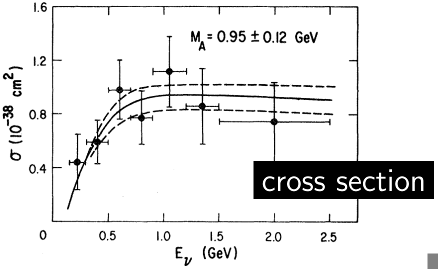

$\nu - D$

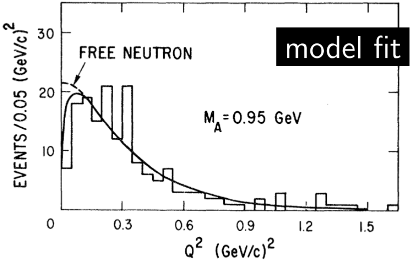

Measurements with heavier targets

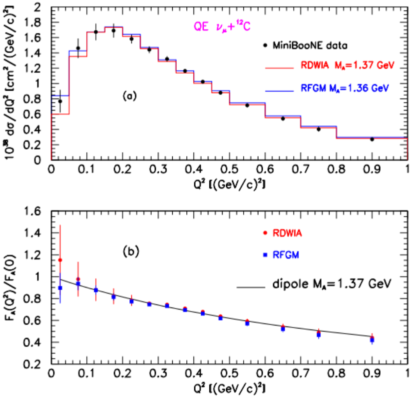

MiniBooNE QE measurement
Aguilar-Arevalo et al., 2010[7]
Butkevich and Perevalov, 2013[8]

- MiniBooNE – inclusive, lepton-only measurement – interpreted as F_{A} on carbon, insensitive to lepton-hadron correlation.

Measurements with heavier targets

MINERνA ν_μ QE measurement

Fiorentini et al.,2013[9]

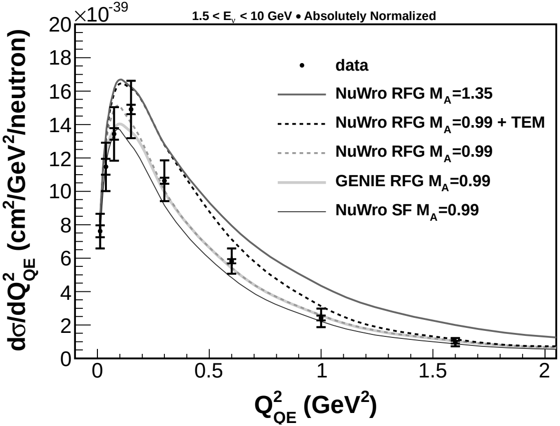

- MiniBooNE – inclusive, lepton-only measurement – interpreted as F_A on carbon, insensitive to lepton-hadron correlation.
- MINERνA QE results: disagree with $M_A = 1.35\ \mathrm{GeV}/c^2$
  - Tension points to nuclear effects.

Measurements with heavier targets

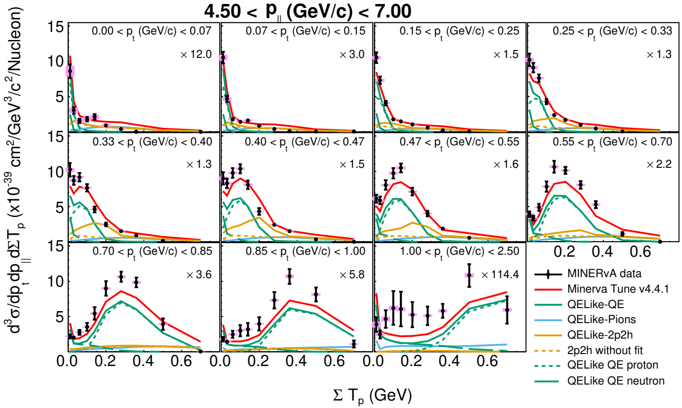

Muon $p_{\parallel}$ vs muon p_t vs total proton kinetic energy
MINERνA Ruterbories et al., 2022[10]

- MiniBooNE – inclusive, lepton-only measurement – interpreted as F_{A} on carbon, insensitive to lepton-hadron correlation.
- MINERνA QE results: disagree with $M_A = 1.35\ \mathrm{GeV}/c^2$
  - Tension points to nuclear effects.
- Better able to identify nuclear effects with lepton-hadron correlations.

Many materials, many models

Important for oscillation measurements

Physics of neutrino cross sections

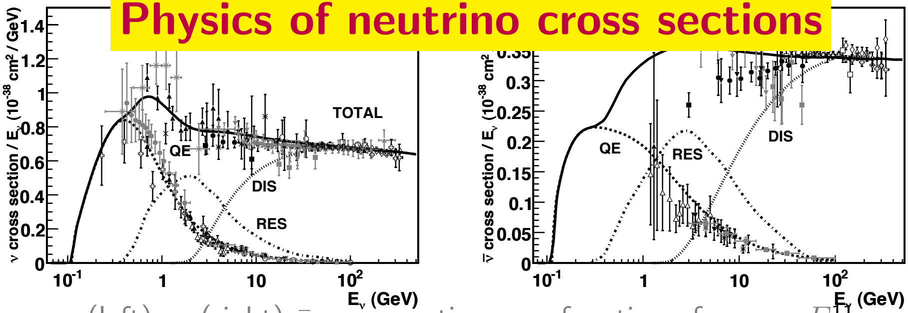

(left) ν, (right) $\bar{\nu}$ cross section as a function of energy E[11]

Rationale for reweighting GENIE relativistic Fermi gas (RFG) model to NuWro's spectral function (SF) model.

Low energy era measurement: MINERνA developed a set of *transverse kinematics imbalance* techniques for the neutrino sample:

- Events with only a primary muon, at least one proton, and no mesons.
- Compare momentum imbalance between μ and p.
- δp_{Ty} measures whether $\vec{p}^{\mu} + \vec{p}^{\mathrm{p}}$ balance out along the $\vec{p}_T^{\mu}$ axis.

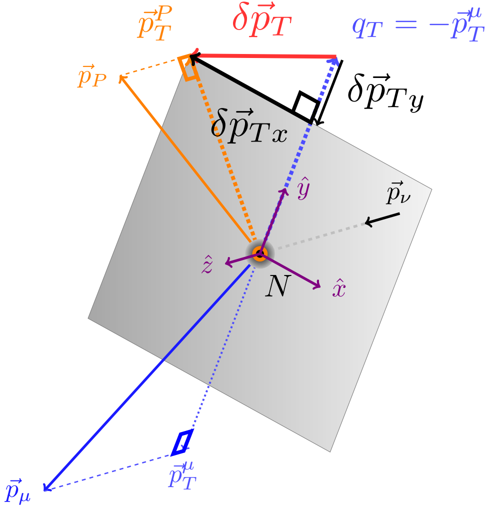

Cai et al., 2019[12]

Low energy era measurement: MINERνA developed a set of *transverse kinematics imbalance* techniques for the neutrino sample:

- Events with only a primary muon, at least one proton, and no mesons.
- Compare momentum imbalance between μ and p.
- δp_{Ty} measures whether $\vec{p}^{\mu} + \vec{p}^{\mathrm{p}}$ balance out along the $\vec{p}^{\mu}_{T}$ axis.
- NuWro spectral function (solid blue) better describes data.

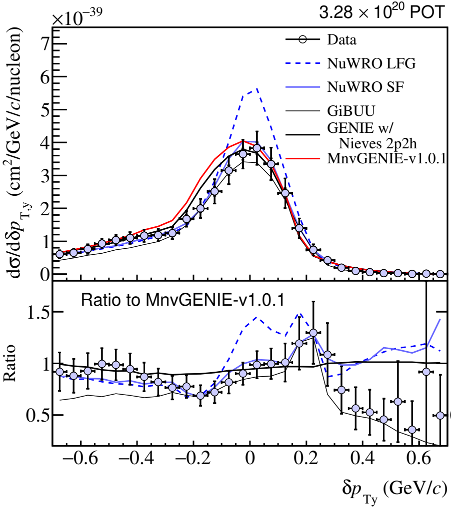

Cai et al., 2019[12]

Blobbing algorithm

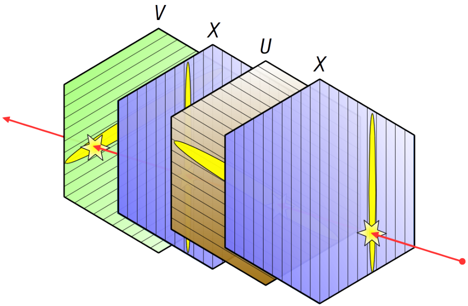

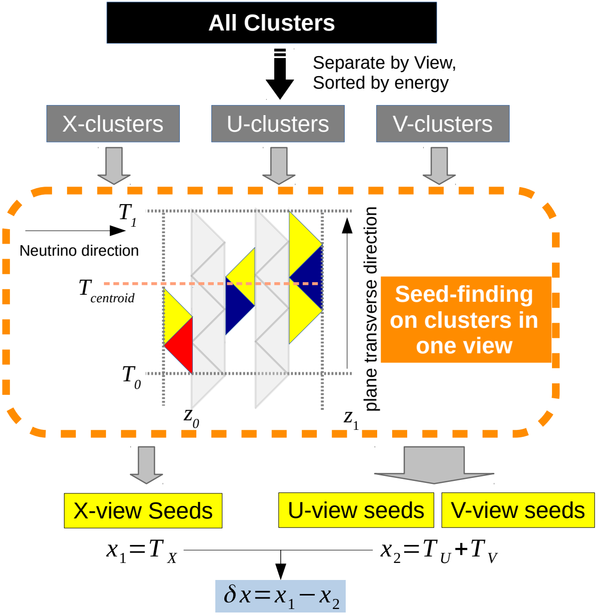

Blobbing algorithm

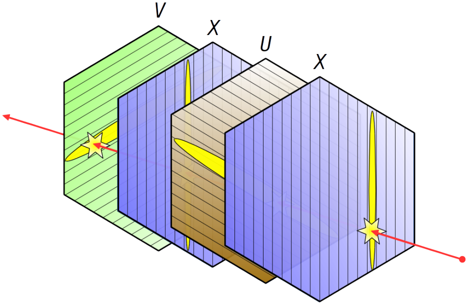

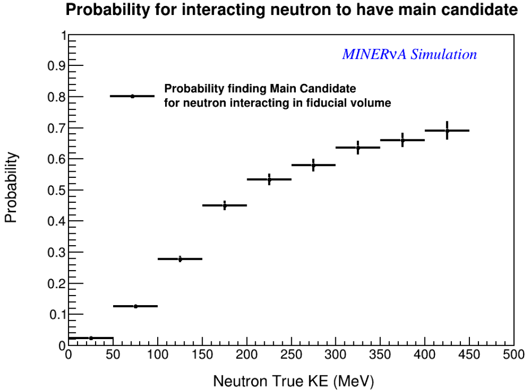

Constraining MINERνA's GEANT4 neutron model with external data.

Plot from reference[13]

Neutron model from Modular Neutron Array (MoNA)

- The MoNA collaboration collected (Del Guerra, 1976[14]) and modeled (Kohley et al., 2012[13]) neutron cross section on CH.
- $^{12}C(n,np)^{11}B$ the dominant interaction channel
- We tune each channel to the MoNA cross sections based on secondary daughter particles.

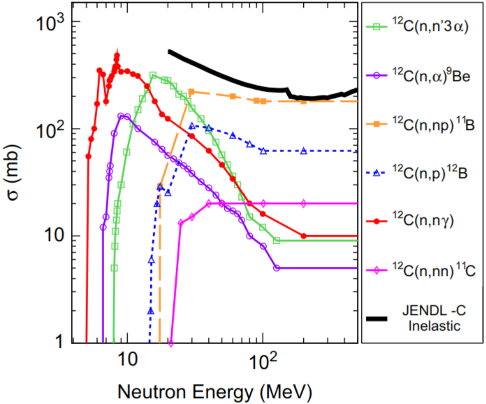

Fig. 3. Inelastic neutron–carbon reaction cross-sections are shown as a function of the incident neutron energy. MENATE_R uses the six different discrete reaction channel cross-sections while the G4-Physics uses the total inelastic reaction cross-sections taken from the JENDL-HE library [37].

GEANT4 reweight – nuisance variables

- We looked at "nuisance" variables to see if the MONA data improved the data/MC agreement
- These variables are not used in the fit and not tuned
- Example includes energy of neutron candidates, and distance of the candidate to vertex
- will show neutron candidate energy deposits in each Q^2_{QE} bin.

Neutron candidate energy deposits vs Q^2_{QE}
Without MoNA.

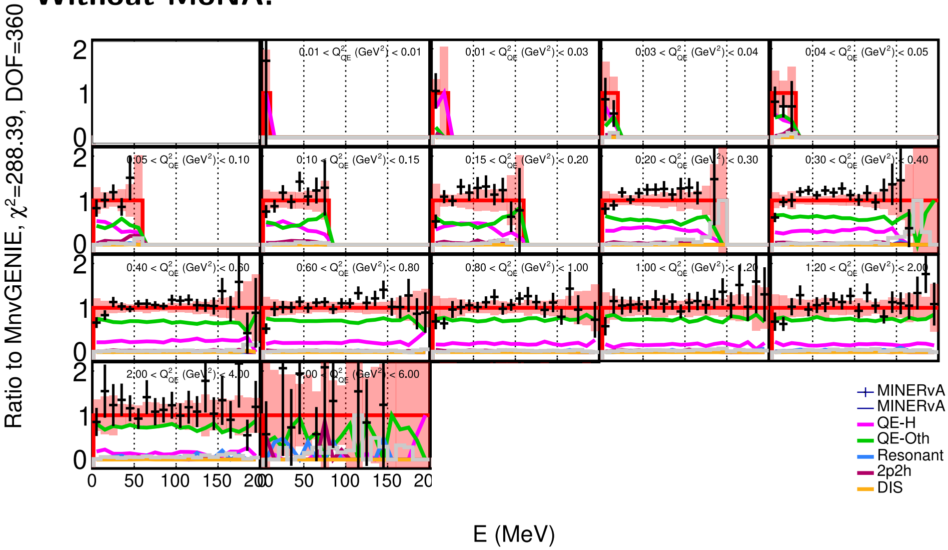

Neutron candidate energy deposits vs Q^2_{QE}

With MoNA: improved χ^2.

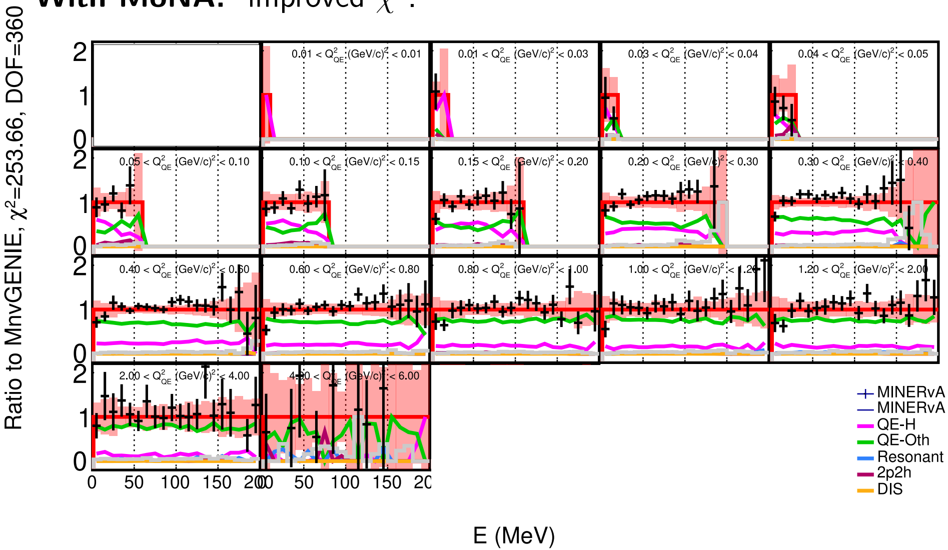

Background constraint method

MC cateogries (**C**) with significant contributions in each Q^2_{QE} bin and angular region is used as template. QELike: CCQE, 2p2h, resonant. Non-QELike: π^0, $\pi^\pm$.

$$\chi^2 = \sum_{S,i} \frac{\left(\left[\sum_C w_{C,i} N^{\mathrm{mc}}_{C,S,i}\right] - N^{\mathrm{data}}_{S,i}\right)^2}{N^{\mathrm{data}}_{S,i}} + \quad \chi^2 \text{ term}$$

$$\lambda_S \sum_C \sum_{j=1}^{N-2} (w_{C,j} + w_{C,j+2} - 2w_{C,j+1})^2. \quad \text{regularizaton term}$$

S: sideband – angular regions participating in fit. **i**: Q^2_{QE} bin. $\mathbf{w}$: Weight for each category in each bin.

λ_{S} controls the strength of the regularization, affects smoothness of the fit, and obtained through an L-curve style scan.

Validating background constraint method with neutrino sample

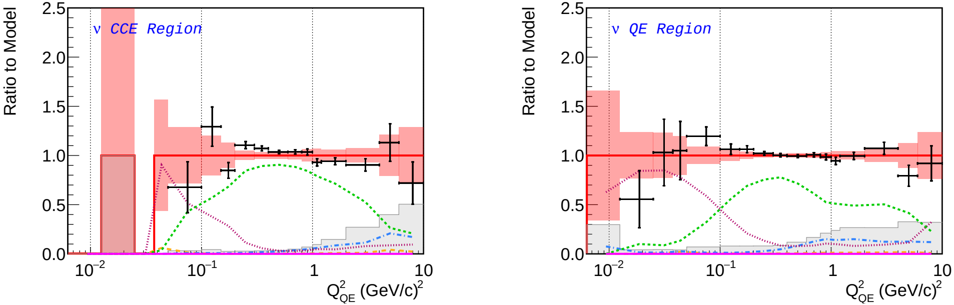

We select events with trackable protons in a **neutrino sample**. Different final states and available kinematics. Apply same fitting mechanism. Data and MC agree within uncertainty except $Q^2 \in (0.2, 0.4)(\mathrm{GeV}/c)^2$.

Validating background constraint method with neutrino sample

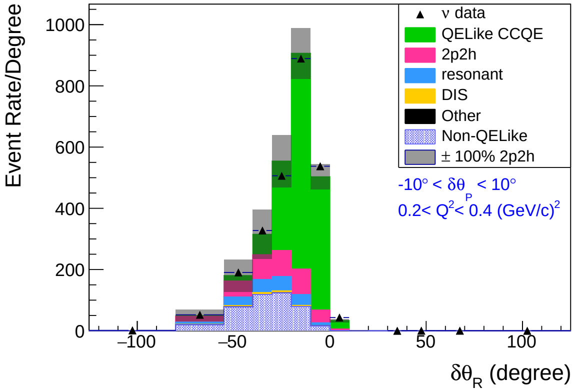

Neutrino mode:

- 100% 2p2h uncertainty covers data/simulation discrepancy.

Antineutrino mode:

- Small 2p2h contribution.
- Sufficiently covered by total uncertainty.

Explanation of the Weights

The CCQE weight is affected by

- Base GENIE model
- Various model tunes:
  - RPA, NuWro SF
- Final state tunes:
  - FSI tunes

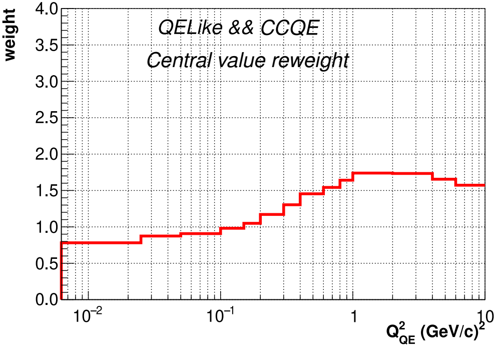

Non-QE **validation region 1** – fitted

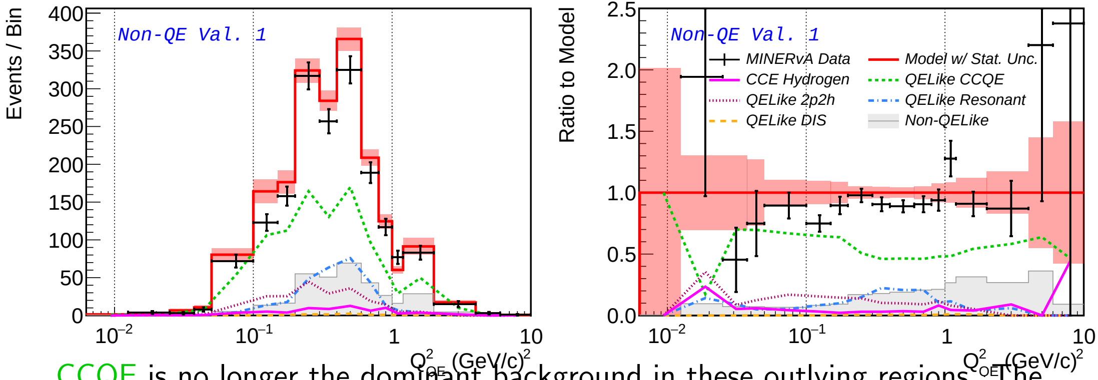

CCQE is no longer the dominant background in these outlying regions. The Non-QE validation regions are mechanically separated into two sub-regions but has smaller effect on the parameter scan due to low statistics.

Non-QE **validation region 2** – fitted

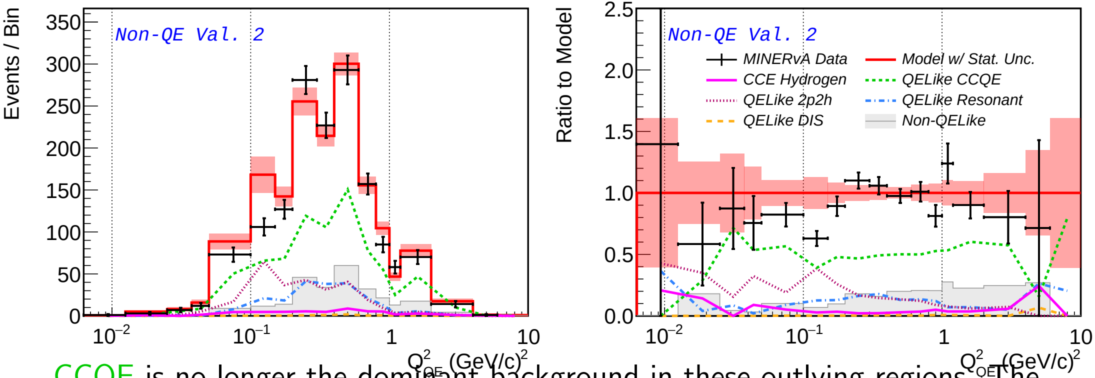

CCQE is no longer the dominant background in these outlying regions. The Non-QE validation regions are mechanically separated into two sub-regions but has smaller effect on the parameter scan due to low statistics.

Non-QE **fit region** – fitted

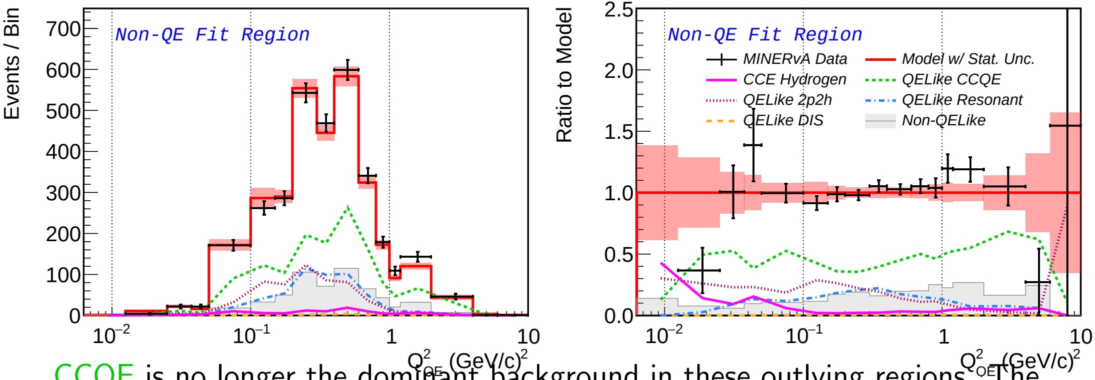

CCQE is no longer the dominant background in these outlying regions. The Non-QE validation regions are mechanically separated into two sub-regions but has smaller effect on the parameter scan due to low statistics.

Non-QE meson **fit region** – fitted

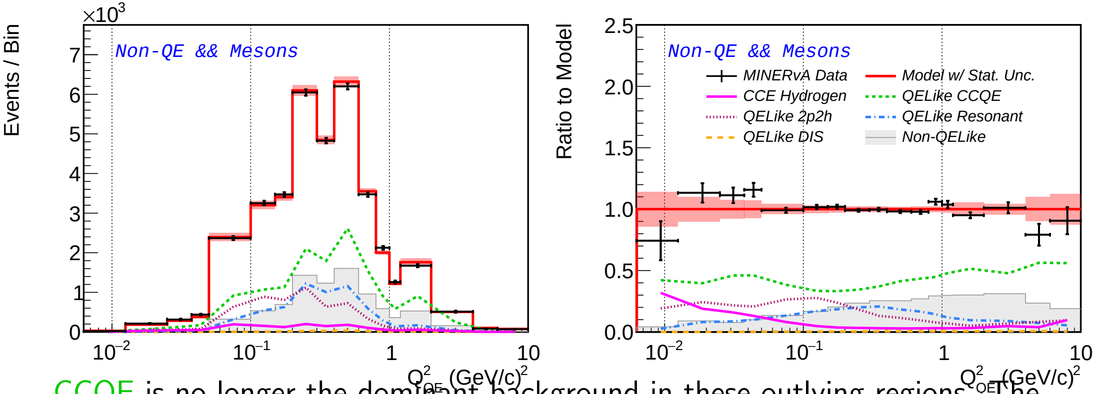

CCQE is no longer the dominant background in these outlying regions. The Non-QE validation regions are mechanically separated into two sub-regions but has smaller effect on the parameter scan due to low statistics.

Effects of background constraint on angular regions

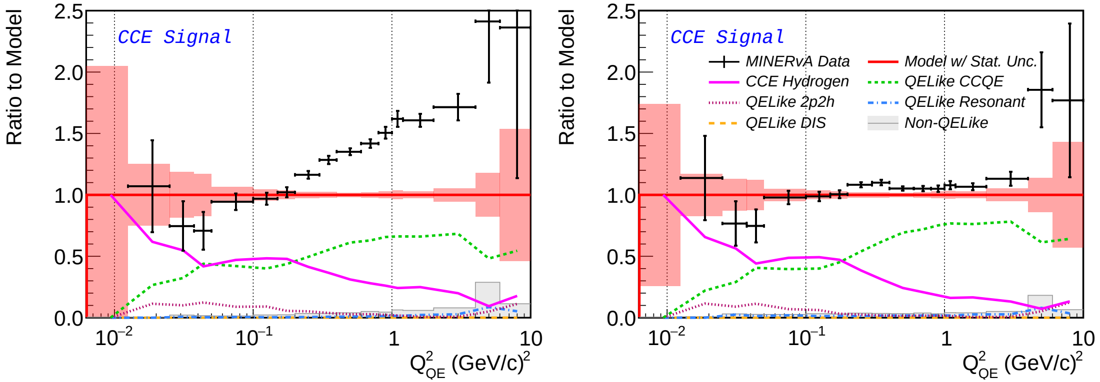

CCE signal region

Ratio of data to (left) unfitted model, (right) post-fitted model.

Effects of background constraint on angular regions

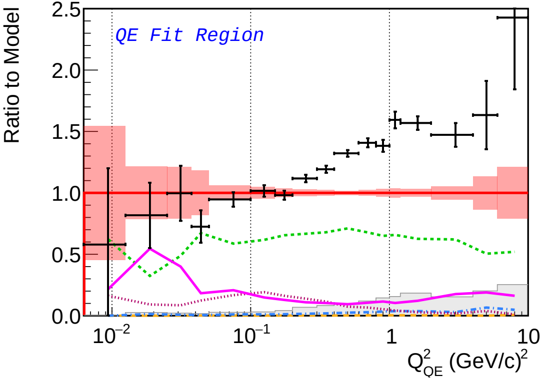

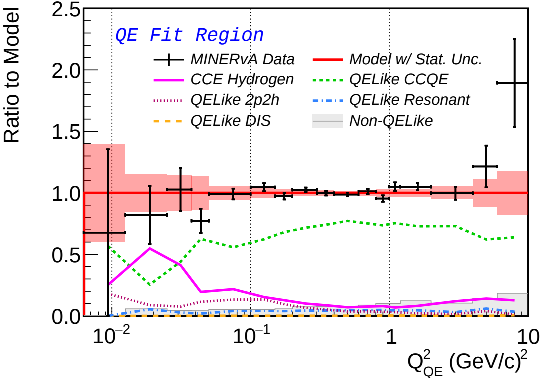

QE fit region

Ratio of data to (left) unfitted model, (right) post-fitted model.

Effects of background constraint on angular regions

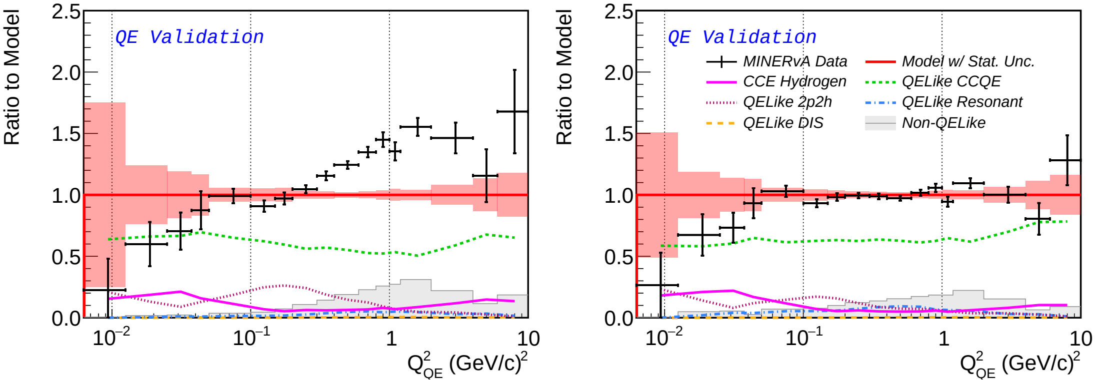

QE validation region

Ratio of data to (left) unfitted model, (right) post-fitted model.

Effects of background constraint on angular regions

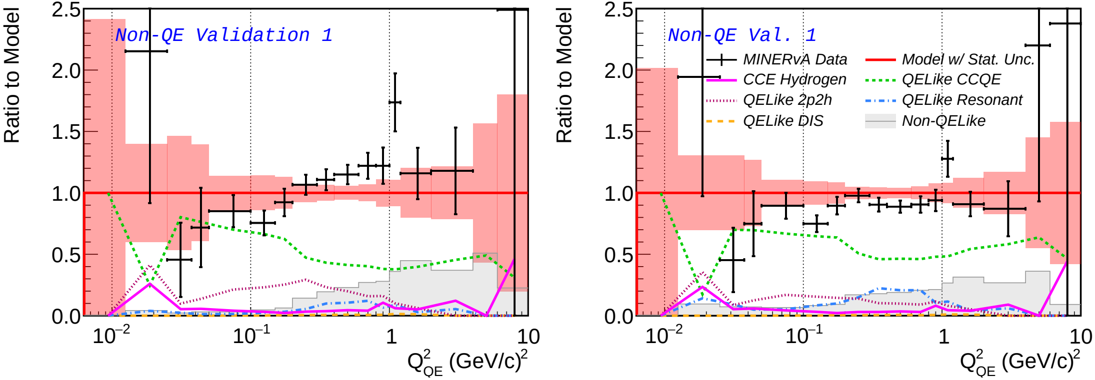

Non-QE validation 1

Ratio of data to (left) unfitted model, (right) post-fitted model.

Effects of background constraint on angular regions

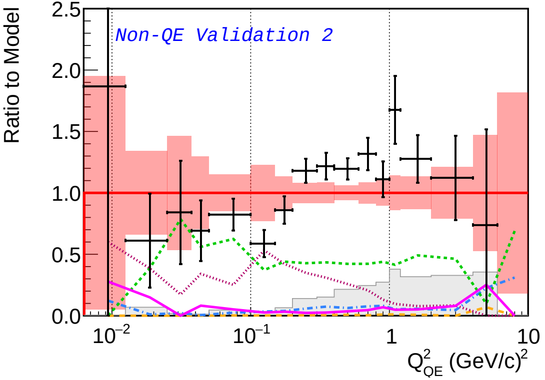

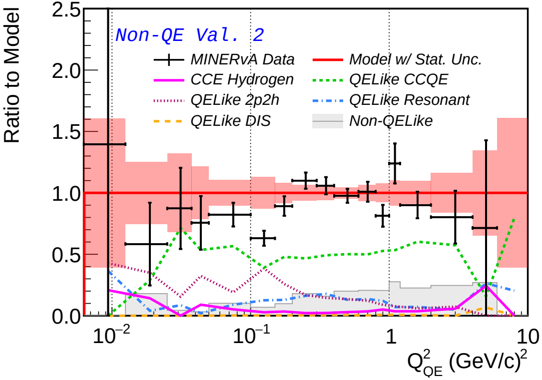

Non-QE validation 2

Ratio of data to (left) unfitted model, (right) post-fitted model.

Effects of background constraint on angular regions

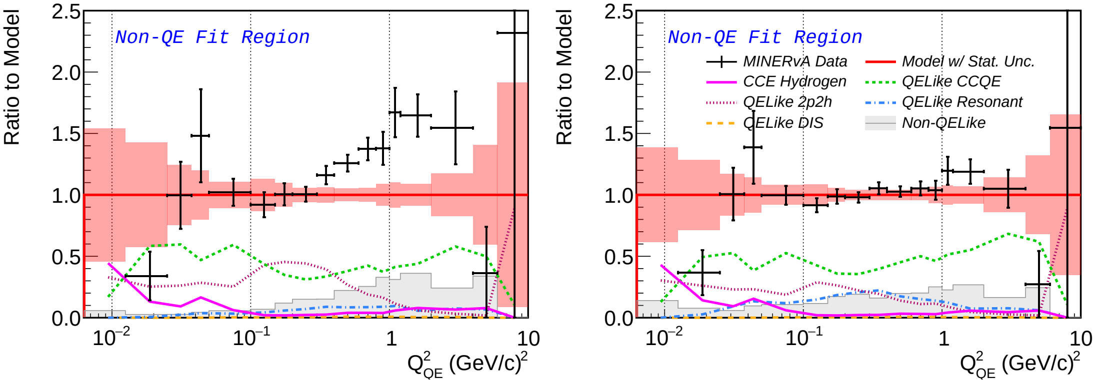

Non-QE fit region

Ratio of data to (left) unfitted model, (right) post-fitted model.

Effects of background constraint on angular regions

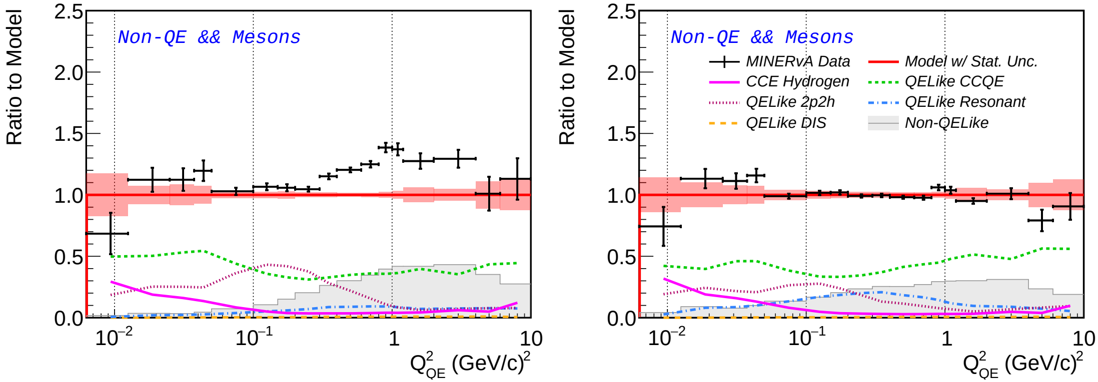

Non-QE and mesons fit region

Ratio of data to (left) unfitted model, (right) post-fitted model.

MINERvA $\bar{\nu}_\mu$-CH result – ratio of data to base model

Bashyal et al., 2022[15]

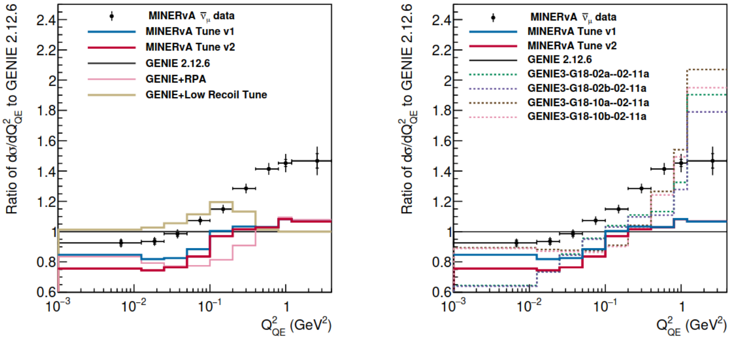

FIG. 4. Comparisons of the cross section predicted by various tunes applied on GENIE with respect to the baseline GENIE 2.12.6 (black) as a function of Q^2_{QE} (left). MINERvA Tune v1 (blue) is the standard simulation tuned to the MINERvA low energy data. MINERvA Tune v2 (red) is MINERvA Tune v1 with the non-resonant pions suppressed in the low Q^2_{QE} region [30]. The remaining curves show the effect of enabling different corrections to the base model. The plots on the right show comparisons of cross sections predictions for GENIE v3.0.6 (dotted lines) with the MINERvA tuned GENIE predictions.Inner ticks in the data are statistical and the outer ticks are the systematic uncertainties.

Migration matrix and warping study

Row normalized migration matrix:
Unfolding matrix obtained by

- D'Agostini iterative unfolding – stops at 4th iteration.

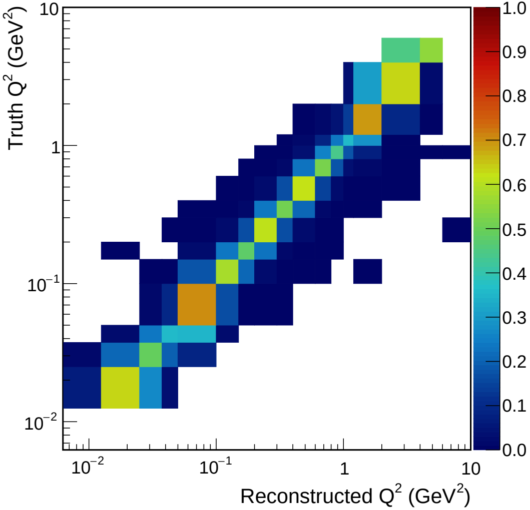

Migration matrix and warping study

Ratio of "warped prediction" to base prediction.

- Performed warping study to check stability of regularization.
- "Warped" prediction with ratio, and
- and generated ensemble of 1000 statistical variations.
- Obtain average and median χ^2 between unfolded and truth of the ensemble for each iteration.

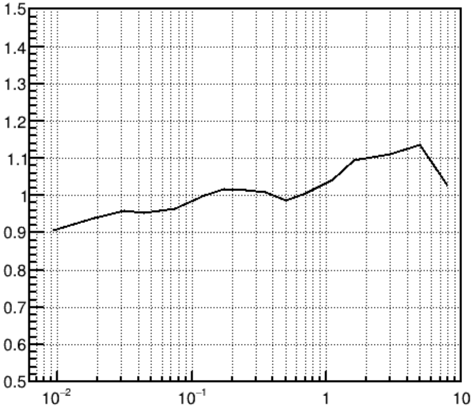

Systematics Uncertainties

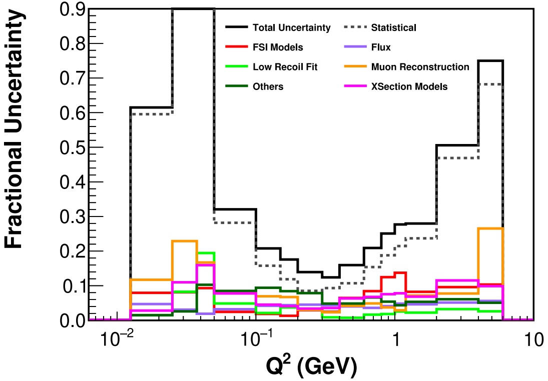

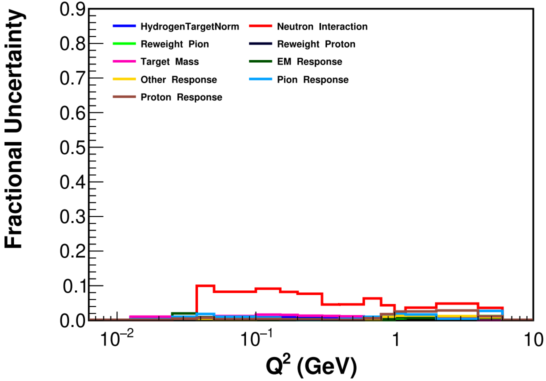

(left) all systematics, (right) others

Systematics Uncertainties

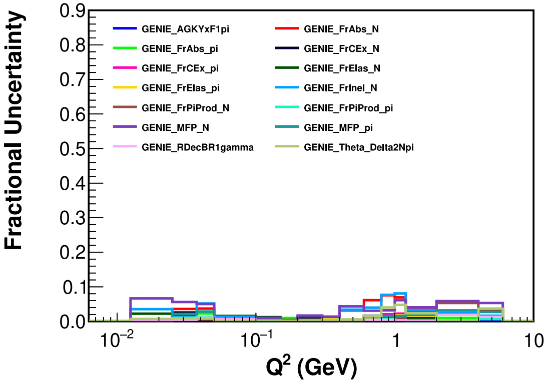

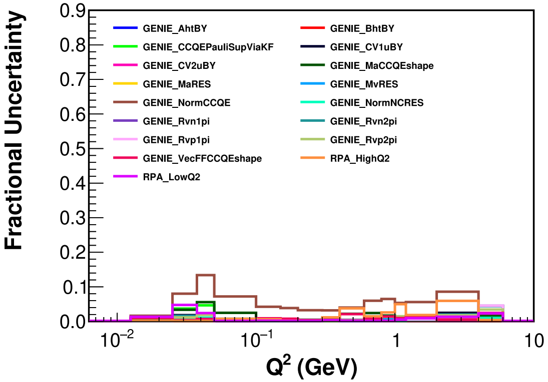

(left) FSI model, (right) cross section model

Systematics Uncertainties

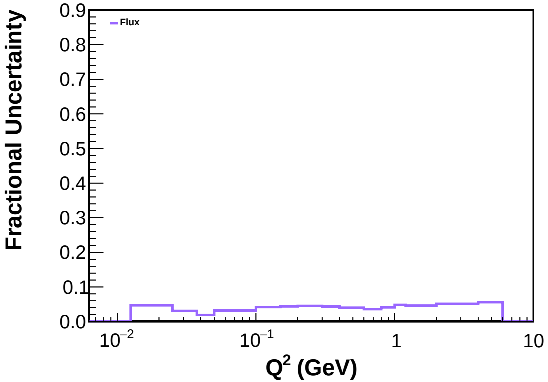

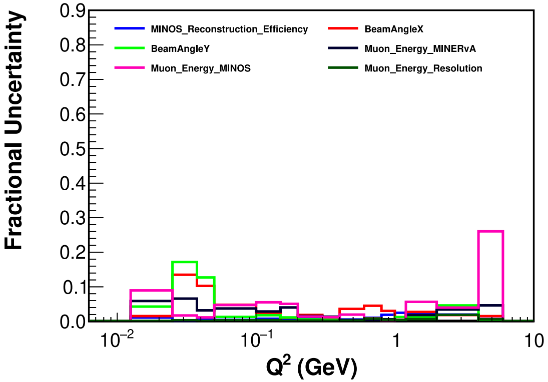

(left) flux, (right) muon reconstruction

Systematics Uncertainties

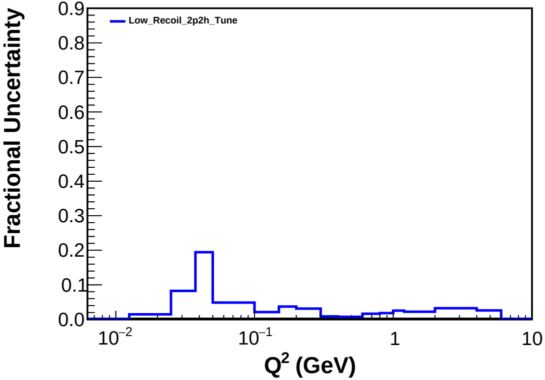

low recoil fit

Neutron secondary scattering

- Ejected protons responsible for majority of secondary neutron interactions.
- Inelastic scattering from carbon dominates (see previous slide)
- MINERνA doesn't have access to the most updated GEANT4 because we need to access MINOS.

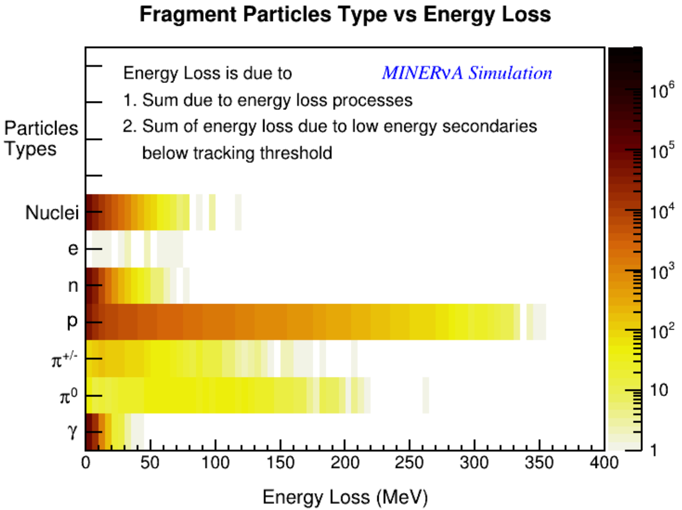

Effect of MONA Reweight – Blob Energy

Without MoNA

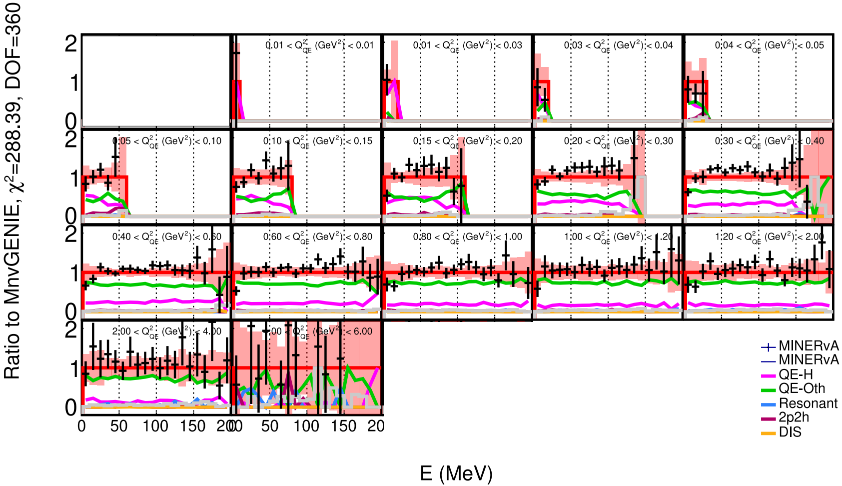

Effect of MONA Reweight – Blob Energy

With MoNA

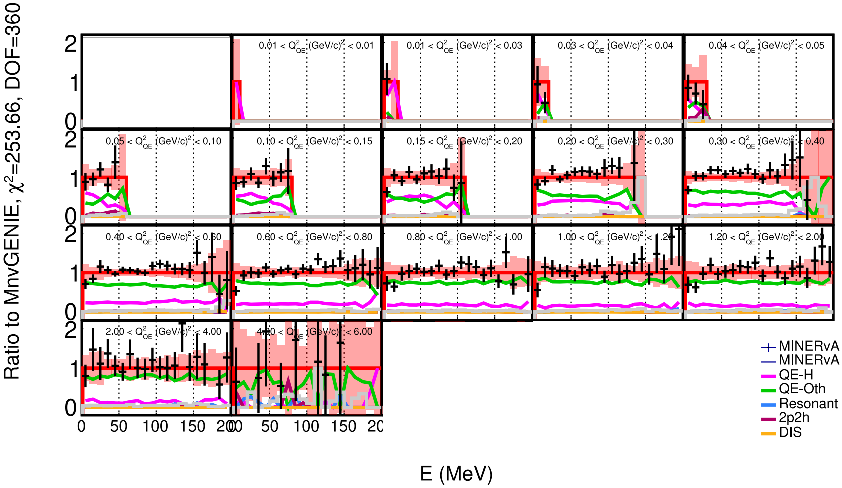

Effect of MONA Reweight – Blob Distance to Vertex

Without MoNA

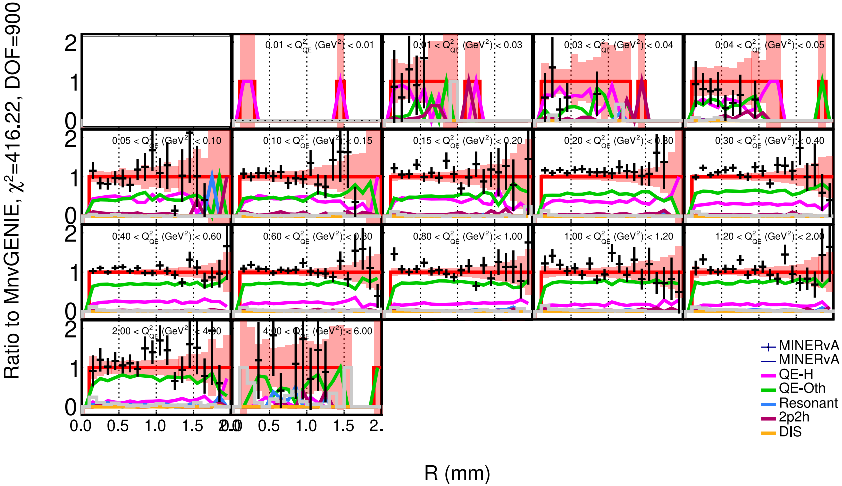

Effect of MONA Reweight – Blob Distance to Vertex

With MoNA

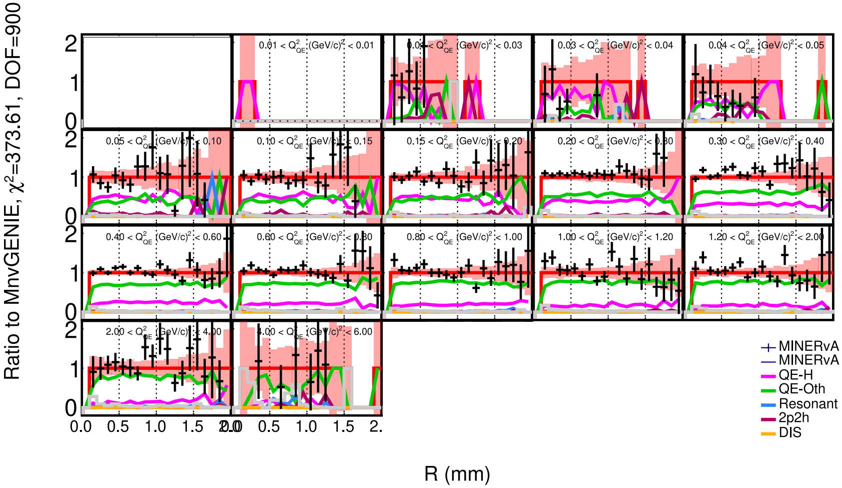

z-expansion parameters

z-expansion formalism and constraints on a_k

$$F_{\mathrm{A}}(Q^2) = \sum_{k=0}^{k_{\mathrm{max}}} a_k z^k$$

$$z = \frac{\sqrt{t_{\mathrm{cut}} + Q^2} - \sqrt{t_{\mathrm{cut}} - t_0}}{\sqrt{t_{\mathrm{cut}} + Q^2} + \sqrt{t_{\mathrm{cut}} - t_0}}$$

$$\sum_{k=n}^{\infty} k(k-1)\dots(k-n+1)a_k = 0, n \in (0,1,2,3)$$

$$\chi^2 = \Delta X \cdot \mathrm{cov}^{-1} \cdot \Delta X + \lambda \left[\sum_{k=1}^{5} \left(\frac{a_k}{5a_0} \right)^2 + \sum_{k=5}^{k_{\mathrm{max}}} \left(\frac{k a_k}{25 a_0} \right)^2 \right]$$

$$\Delta X = \mathrm{data} - \mathrm{prediction}$$

z-expansion parameters II

Central value fit: $k_{\max} = 8, \lambda = 0.13$

- Scan through large range of λ
- Data χ^2 for $k_{\max} = 8$ can be less than $k_{\max} = 6$
- λ chosen at point of maximum curvature.

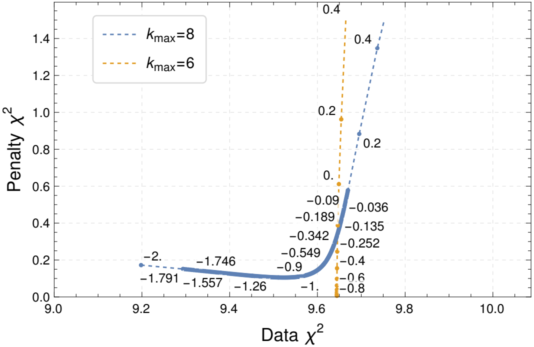

Dipole Fit

- $M_A = 1.15(10)$ GeV
- Fit $\chi^2 = 10.2$
- Comparable with z-expansion fit
  - $k_{\max} = 6$
  - $\lambda = 0$
  - $\chi^2 = 9.64$

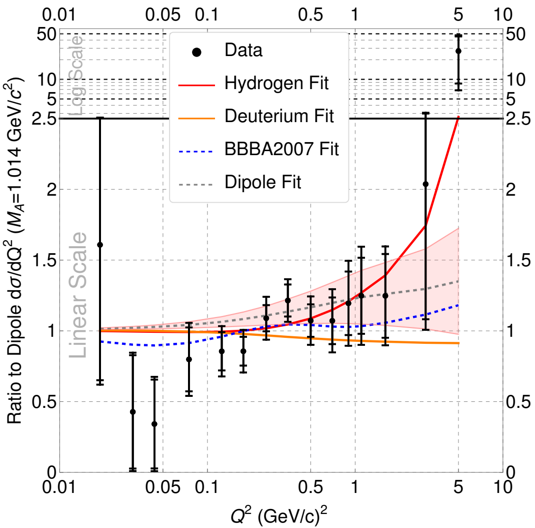

Changing GENIE's initial state model

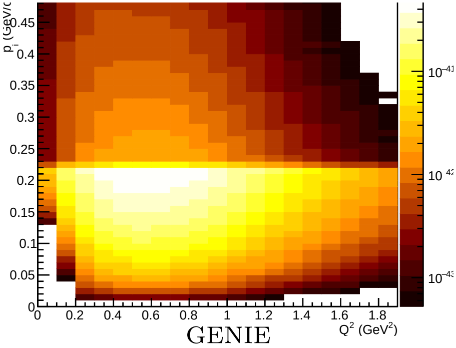

→

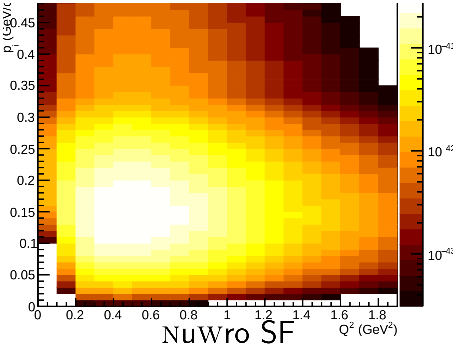

Transform GENIE RFG to NuWro SF
in $|p_i| - Q^2$ space

Relativistic Fermi Gas (RFG), Local Fermi Gas (LFG) and Spectral Function (SF)

- RFG: non-interacting fermions in a potential well with fixed Fermi momentum K_F.
- GENIE RFG includes an additional tail.
- LFG: Fermi gas with location-dependent K_F.
- SF: a nuclear-shell model.

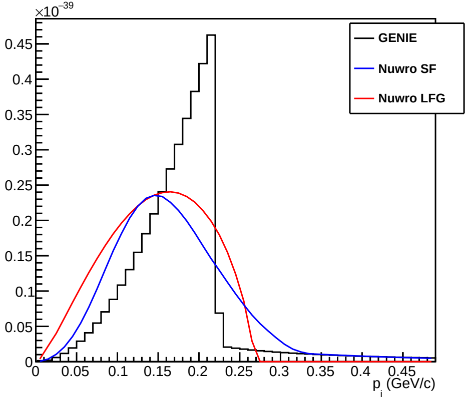

Initial state momentum distribution.

F_{A} fit and axial radius of the nucleon

Favors larger F_{A} at higher Q^2.

Calculate proton radius from F_{A} for $Q^2 \to 0$.

$$F_{\mathrm{A}}(Q^2) = F_{\mathrm{A}}(0)\left(1 - \frac{\langle r_A^2\rangle}{3!}Q^2 + \frac{\langle r_A^4\rangle}{5!}Q^4 + \dots\right),$$

$$\frac{1}{F_{\mathrm{A}}(0)}\frac{\mathrm{d}F_{\mathrm{A}}}{\mathrm{d}Q^2}\bigg|_{Q^2=0} = -\frac{1}{6}\langle {r_A}^2\rangle$$

- $\langle r_A^2\rangle = 0.53(25)\mathrm{fm}^2$
- $\sqrt{\langle r_A^2\rangle} = 0.73(17)\mathrm{fm}$

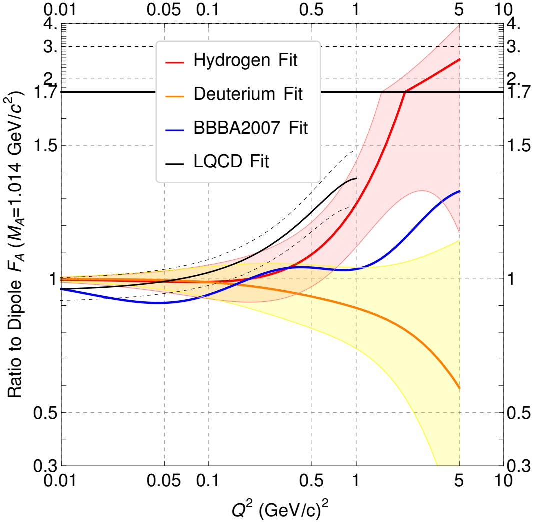

F_A fit and axial radius of the nucleon

Favors larger F_A at higher Q^2.
Calculate proton radius from F_A for $Q^2 \to 0$.

$$F_A(Q^2) = F_A(0)\left(1 - \frac{\langle r_A^2\rangle}{3!}Q^2 + \frac{\langle r_A^4\rangle}{5!}Q^4 + \dots\right),$$

$$\frac{1}{F_A(0)}\frac{dF_A}{dQ^2}\bigg|_{Q^2=0} = -\frac{1}{6}\langle {r_A}^2\rangle$$

- $\langle r_A^2\rangle = 0.53(25)\mathrm{fm}^2$
- $\sqrt{\langle r_A^2\rangle} = 0.73(17)\mathrm{fm}$

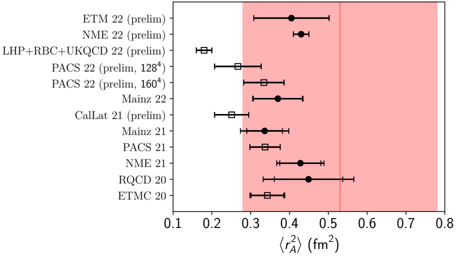

Filled circle: full error budget.
Open square: incomplete.
Red band: this result.
Courtesy of Aaron Meyer.

Reference

Reference I

[1] Aaron S. Meyer, André Walker-Loud, and Callum Wilkinson. "Status of Lattice QCD Determination of Nucleon Form Factors and their Relevance for the Few-GeV Neutrino Program". In: (Jan. 2022). DOI: 10.1146/annurev-nucl-010622-120608. arXiv: 2201.01839 [hep-lat].

[2] R. Bradford et al. "A New parameterization of the nucleon elastic form-factors". In: *Nucl. Phys. B Proc. Suppl.* 159 (2006). Ed. by F. Cavanna, J. G. Morfin, and T. Nakaya, pp. 127–132. DOI: 10.1016/j.nuclphysbps.2006.08.028. arXiv: hep-ex/0602017.

[3] Aaron S. Meyer et al. "Deuterium target data for precision neutrino-nucleus cross sections". In: *Phys. Rev. D* 93.11 (2016), p. 113015. DOI: 10.1103/PhysRevD.93.113015. arXiv: 1603.03048 [hep-ph].

Reference II

[4] A. Bodek et al. "Vector and Axial Nucleon Form Factors:A Duality Constrained Parameterization". In: *Eur. Phys. J. C* 53 (2008), pp. 349–354. DOI: 10.1140/epjc/s10052-007-0491-4. arXiv: 0708.1946 [hep-ex].

[5] Huey-Wen Lin. "Nucleon helicity generalized parton distribution at physical pion mass from lattice QCD". In: *Phys. Lett. B* 824 (2022), p. 136821. DOI: 10.1016/j.physletb.2021.136821. arXiv: 2112.07519 [hep-lat].

[6] W. A. Mann et al. "Study of the reaction nu n —> mu- p". In: *Phys. Rev. Lett.* 31 (1973), pp. 844–847. DOI: 10.1103/PhysRevLett.31.844.

Reference III

[7] A. A. Aguilar-Arevalo et al. "First Measurement of the Muon Neutrino Charged Current Quasielastic Double Differential Cross Section". In: *Phys. Rev. D* 81 (2010), p. 092005. DOI: 10.1103/PhysRevD.81.092005. arXiv: 1002.2680 [hep-ex].

[8] A. V. Butkevich and D. Perevalov. "Determination of the Axial Nucleon Form Factor from the MiniBooNE Data". In: *Phys. Rev. D* 89.5 (2014), p. 053014. DOI: 10.1103/PhysRevD.89.053014. arXiv: 1311.3754 [hep-ph].

[9] G. A. Fiorentini et al. "Measurement of Muon Neutrino Quasielastic Scattering on a Hydrocarbon Target at $E_\nu \sim 3.5$ GeV". In: *Phys. Rev. Lett.* 111 (2013), p. 022502. DOI: 10.1103/PhysRevLett.111.022502. arXiv: 1305.2243 [hep-ex].

Reference IV

[10] D. Ruterbories et al. "Simultaneous Measurement of Proton and Lepton Kinematics in Quasielasticlike $\nu\mu$-Hydrocarbon Interactions from 2 to 20 GeV". In: *Phys. Rev. Lett.* 129.2 (2022), p. 021803. DOI: 10.1103/PhysRevLett.129.021803. arXiv: 2203.08022 [hep-ex].

[11] J. A. Formaggio and G. P. Zeller. "From eV to EeV: Neutrino cross sections across energy scales". In: *Rev. Mod. Phys.* 84 (3 Sept. 2012), pp. 1307–1341. DOI: 10.1103/RevModPhys.84.1307. URL: https://link.aps.org/doi/10.1103/RevModPhys.84.1307.

[12] T. Cai et al. "Nucleon binding energy and transverse momentum imbalance in neutrino-nucleus reactions". In: *Phys. Rev. D* 101.9 (2020), p. 092001. DOI: 10.1103/PhysRevD.101.092001. arXiv: 1910.08658 [hep-ex].

Reference V

[13] Z. Kohley et al. "Modeling interactions of intermediate-energy neutrons in a plastic scintillator array with Geant4". In: *Nuclear Instruments and Methods in Physics Research Section A: Accelerators, Spectrometers, Detectors and Associated Equipment* 682 (2012), pp. 59–65. ISSN: 0168-9002. DOI: https://doi.org/10.1016/j.nima.2012.04.060. URL: https://www.sciencedirect.com/science/article/pii/S0168900212004329.

[14] A. Del Guerra. "A compilation of n-p and n-C cross sections and their use in a Monte Carlo program to calculate the neutron detection efficiency in plastic scintillator in the energy range 1–300 MeV". In: *Nuclear Instruments and Methods* 135.2 (1976), pp. 337–352. ISSN: 0029-554X. DOI: https://doi.org/10.1016/0029-554X(76)90181-6. URL: https://www.sciencedirect.com/science/article/pii/0029554X76901816.

Reference VI

[15] A. Bashyal et al. “High-Statistics Measurement of Antineutrino Quasielastic-like scattering at $E_\nu \sim 6$~GeV on a Hydrocarbon Target”. In: (Nov. 2022). arXiv: 2211.10402 [hep-ex].